PCCP

Crucial Role of Electron Transfer from Interfacial Molecules in Negative Potential Shift of Au Electrode Immersed in Ionic Liquid

Journal:	*Physical Chemistry Chemical Physics*
Manuscript ID	CP-ART-07-2018-004594.R1
Article Type:	Paper
Date Submitted by the Author:	07-Oct-2018
Complete List of Authors:	Inagaki, Taichi; Nagoya University, Graduate School of Informatics Takenaka, Norio; Nagoya University, Graduate School of Informatics Nagaoka, Masataka; Nagoya University, Graduate School of Informatics

Crucial Role of Electron Transfer from Interfacial Molecules in Negative Potential Shift of Au Electrode Immersed in Ionic Liquid

Taichi Inagaki[*†], Norio Takenaka[†‡], and Masataka Nagaoka[*†‡§]

[†]*Graduate School of Informatics, Nagoya University, Furo-cho, Chikusa-ku, Nagoya 464-8601, Japan*

[‡]*Elements Strategy Initiative for Catalysts and Batteries (ESICB), Kyoto University, Nishikyo-ku Kyoto 615-8510, Japan*

[§] *Core Research for Evolutional Science and Technology, Japan Science and Technology Agency, Honmachi, Kawaguchi 332-0012, Japan*

E-mail: inagaki@ncube.human.nagoya-u.ac.jp; mnagaoka@i.nagoya-u.ac.jp

Phone: +81 (0)52 789 5623. Fax: +81 (0)52 789 5623

Abstract:

Potential of zero charge (PZC) is essential in electrochemistry to understand physical and chemical phenomena at the interface between an electrode and a solution. A negative potential shift from the work function to the PZC has been experimentally observed in the metal/ionic liquid (IL) system, but the mechanism remains unclear and controversial. In this paper we provide valuable insight into the mechanism on the potential shift in the Au/IL (1-butyl-3-methylimidazolium bis(trifluoromethanesulfonyl)amide: [BMIM][TFSA]) system using a computational approach combining classical molecular dynamics simulations and first-principles calculations. By separately estimating some contributions to the potential shift, the shift is calculated in an easy-to-understand manner. The resultant PZC is shown to be in good agreement with the experimental one. Among the contributions, the electron redistribution at the Au/IL interface is found to provide the largest negative potential change. This indicates that the redistribution plays a crucial role to determine the potential shift of the Au electrode immersed in the IL. The detailed analyses suggest that the redistribution corresponds to the electron transfer not only from the anionic TFSA but also from the cationic BMIM molecules to the Au electrode surface. This unique observation is understood to originate from the interfacial structure where the IL molecules are in very close proximity to the electrode surface via the dispersion interaction.

1 Introduction:

Electrode potential is a fundamental physical quantity in electrochemistry. In particular, the rest potential in the situation where the electrode has no excess charge is defined as the potential of zero charge (PZC). The PZC is often used as a reference point to investigate the potential dependence of electrode/solution interfacial phenomena, as it is commonly reported that cations adsorb on the electrode surface with lower potential than the PZC and vice versa. In addition, the PZC also plays an essential role to characterize the electrode/electrolyte interfacial structure as typified by the electrical double layer.[1] Since the PZC is influenced not only by electronic structure of the metal electrode but also by orientation of ions and molecules at the interface, it can furthermore be useful for understanding dynamical features like interfacial chemical reactions including charge transfer processes.[2-6] Many practical applications in electrochemistry such as batteries, electrochemical capacitors, chemical sensors, and molecular electronic devices are, accordingly, strongly connected to the variation of the PZC.[7–10] This indicates that the PZC determination provides meaningful information in electrochemical researches.

The PZC is also related closely to work function of metal in a physical perspective.[11–13] Work function of metal Ψ_M is energy needed to remove an electron from the metal to a point in the vacuum just outside its surface. On the other hand, according to the general definition of absolute electrode potential,[14] PZC (or electrode potential) is a potential level of an electron in the metal immersed in a solution with reference to a point in the vacuum just outside the solution. In other words, the PZC can be regarded as a work function modified by a solution,[1,15]

$$\Phi_{M/S}(\text{abs}) = \Psi_M / e_0 + \Delta\Psi(M,S), \quad (1)$$

where $\Phi_{M/S}(\text{abs})$ is the PZC of a metal (M) immersed in a solution (S) at the absolute scale, $-e_0$ is the charge of an electron, and $\Delta\Psi(M,S)$ is the potential shift to the PZC. The value of $\Delta\Psi(M,S)$ depends on both the metal and solution species. (Detailed explanations for the term are given in Ref. 15.) Work function and PZC are technical terminologies in surface science and electrochemistry, respectively, but for the easy understanding in this paper the former is defined as a potential (energy) for electrons in the bare metal in *vacuum* and the latter as a potential for electrons in the metal immersed in *solution*.

The potential shift, $\Delta\Psi(M,S)$, has been generally explained with the potential change in the metal interior due to the presence of a solution with reference to the level. Two contributions have been commonly considered for the change: charge (or electron) transfer between the electrode and solution species and orientation of solution species themselves. These effects modify the dipole moment of the system along the normal direction to the electrode surface. The potential shift as well as the two contributions has been investigated extensively using theoretical approaches[16–19] at the microscopic scale. For example, the Pt electrode/water interface has attracted much attention because of the importance in fuel and electrolysis cells. While experiments showed $\Delta\Psi(M,S) \sim -1.1$ V for the Pt(111) immersed in water,[17,20] recent theoretical studies have revealed that the potential shift is attributed mainly to the charge transfer between the Pt electrode and water molecules, rather than the orientation of water molecules. Jinnouchi and Anderson argued that charge redistributions induced by the adsorption of water molecules form a surface dipole moment that dominates the

experimentally observed negative shift in the PZC.[17] The same conclusion has been derived for other metals (such as Au, Pd, and Ag) in the most recent work by Le and coworkers.[18] Thus, in the metal/water systems, the most important effect for $\Delta\Psi(M,S)$ has been understood to be a charge transfer occurred as a result of the interaction between the electrode metal and water molecules at the interface.

Water is not the only solvent that is importantly used in electrochemistry. In recent years, ionic liquids (ILs), which are molten salts usually consisting of organic ions with a melting temperature below about 400 K, have attracted extensive attention as electrolyte solvent. This is because ILs have many unique properties such as high ionic conductivity, electrochemical stability, and low flammability.[21] They thus are investigated for the novel applications to electrochemical devices such as electrical double layer capacitors[22] and Li-ion batteries.[23] Focusing on the electrode potential as in the case of water, it is reported the PZC of the metal electrode immersed in ILs is a result of a large negative potential shift from the work function. For example, Motobayashi and coworkers experimentally showed that an Au electrode, which has the work function of 5.31 eV,[24] has the PZC of 4.1-4.5 V at the absolute scale upon immersing in IL[25,26]. This indicates that a large negative potential shift (~–1 V) is caused by IL. Also for other metal electrodes, there are a few examples of the similar negative potential shift.[27,28] These negative potential shifts are comparable to those in the case of the metal/water systems. According to the understanding in the metal/water system, the negative potential shift in the metal/IL systems is expected to stem from the charge transfer between the electrode and IL molecules. Even if it is true, however, the detailed mechanism is not yet well understood; which molecule (cation or anion or both) releases the electron toward the electrode, how much charge transfer dominates

the potential shift, and what is the essential origin of the potential shift? On the other hand, there are some theoretical studies which suggest that such charge transfer at the interface is unlikely to occur[29,30]. For example, Buchner and coworkers showed that the charges of the cation and the anion hardly change upon adsorption on Ag(111).[29] Besides the charge analysis, they showed quite small electrostatic adsorption energy for supporting their suggestion. As found from the current situation, the mechanism on the potential shift in metal/IL systems remains still unclear and controversial, despite its great importance in many practical applications in electrochemistry.

In this paper, we provide valuable insight into the mechanism on the negative potential shift in a metal/IL system. To make a consistent comparison with the experiment,[25] we consider an Au electrode immersed in ionic liquid of 1-butyl-3-methylimidazolium bis(trifluoromethanesulfonyl)amide ([BMIM][TFSA]). The PZC and potential shift are theoretically estimated in the easy-to-understand manner based on the idea that the potential shift can be measured by the sum of potential changes at interfaces. Details of the method are described in the next section. According to the method, we separately estimate some interfacial potential changes by performing the density functional theory based first-principles calculations. The computed potential changes are used to identify the largest contribution to the negative potential shift, in addition to predicting the computational PZC value. On the basis of the detailed analyses of the electronic structure, we illustrate the crucial nature of electron redistribution at the interface and reveal the essential origin of the potential shift. Finally, the obtained results are used to infer the potential shift behavior in other metal/IL systems and electrochemical conditions.

2 Methods:

2.1 Theoretical method for estimate of potential shift and PZC

To understand the mechanism on the negative potential shift observed in the Au/IL system, the potential shift and the resultant PZC are estimated by using the first-principles calculations. On the straightforward consideration, using a system including both the electrode and a large number of IL molecules, the PZC can be estimated directly from the potential difference between the vacuum level just outside the IL and the Fermi level of the Au electrode. After the estimate of PZC, the potential shift $\Delta\Psi(M,S)$ is obtained by subtracting the work function (Ψ_M/e_0) from the PZC $\Phi_{M/S}$(abs) according to Eq. 1. This direct estimate of PZC is conceptually quite simple, but has two serious drawbacks for our purpose. One is that the underlying mechanism is difficult to understand. This is because it provides only the final resultant value where each contribution is already integrated as most experiments are. The other is that we must treat a whole system including both the electrode and a large number of IL molecules. This leads to a high computational cost in the first-principles calculations. The high cost will become a major obstacle in obtaining the statistically meaningful results comparable to experiments.

We, therefore, employed another way to estimate the potential shift and the PZC in this study. The way is based on the idea that the PZC, i.e., potential difference between the vacuum and the electrode, can be measured by the sum of several potential changes occurring at interfaces and the potential derived from the work function. This idea has been shown in the previous papers[19,31,32] to be appropriate to analyze the total potential shift. By assuming that the three different kinds of potential changes contribute to the potential shift, the PZC is given by

$$\Phi_{M/S}(\text{abs}) = \Psi_M / e_0 + \delta\Psi / e_0 + \delta\phi_{ele} + \delta\phi_{ori}, \quad (2)$$

where the last three terms in the right hand side are the potential changes considered in this study ($\Delta\Psi(M,S) = \delta\Psi/e_0 + \delta\phi_{ele} + \delta\phi_{ori}$). The first term related to the potential shift, $\delta\Psi$, accounts for the effect of geometrical distortions of the electrode surface due to the solvation, which can be expressed by the work function difference between the electrode with a clean surface and that with a geometrically distorted surface (Ψ_{distM}), i.e.,

$$\delta\Psi = \Psi_{distM} - \Psi_M . \quad (3)$$

Note that although this contribution has been rarely considered in the previous studies, it should not be omitted when describing the potential shift adequately[32]. The last two terms $\delta\phi_{ele}$ and $\delta\phi_{ori}$ account, respectively, for the effect of the electron redistribution due to the attachment of IL molecules on the electrode surface and that of the macroscopic orientation of IL molecules. Note that, in the latter term, the electron redistribution (or electronic polarization) effect among IL molecules is also included inherently by using the first-principles calculations. These two potential changes are estimated as potential drops along the normal direction to the electrode surface (i.e., the z direction in this paper)

$$\delta\phi_X = \phi_X(z = z_-) - \phi_X(z = z_+) \quad (\text{X=ele or ori}), \quad (4)$$

where z_- and z_+ stand for the lowest and highest z positions at the computational box edges, respectively. Both edges are in the vacuum, and the position of z_+ is set to the reference point of potential in the present case. It should be noted that the potential ϕ is defined for a positive unit charge, not a negatively charged electron, in this paper. For the estimate of $\delta\phi_X$ there is no need to treat the whole system including both the

electrode and a number of IL molecules. It means that the Au/IL interface and the IL molecular region are su□cient for the estimates of $\delta\phi_{ele}$ and $\delta\phi_{ori}$, respectively. By using this method, it becomes possible to estimate the potential shift in the easy-to-understand manner without costly first-principles calculations with a whole large system. This strategy is quite suitable for our purpose here.

Another critical point to estimate the potential shift appropriately is to take into account the statistical average of a number of IL configurations.[18,33,34] It has been reported in the metal/water cases that the potential shift changes no less than ~2 V depending on the molecular orientation of water at the electrode surface.[6,33] In order to incorporate the statistical e•ect, the classical molecular dynamics (MD) simulation method is employed in this study. Owing to the low computational cost of the method, a number of configurations which are uncorrelated with each other can be obtained more easily than the first-principles MD simulation method. In fact, because of the high viscosity of the IL solution, it seems to be unfeasible to obtain many uncorrelated configurations by using the first-principles MD simulation. Experiments showed that there is no dissociative adsorption of BMIM and TFSA molecules on the Au electrode,[25] which also supports the use of the classical MD simulations.

2.2 Computational details

The whole system used in the classical MD simulations is displayed in Figure 1. This system consists of the Au electrode and IL molecules, which includes three interfaces between the electrode and vacuum, the electrode and the IL, and the IL and vacuum due to the three dimensional periodic boundary conditions. The electrode is represented by three layers of Au atoms in the fcc(111) geometry with the experimental lattice constant (4.078 Å) of bulk Au[35]. The three-layered electrode model is followed in the previous

papers.[17,36,37] There are 30 Au atoms in a layer with $5\times3\sqrt{3}$ unit cell, which results in the surface area in the xy plane of 14.42×14.98 Å^2. In this study, this surface area is preserved throughout all calculations including the first-principles ones. With the same-sized unit cell 20 IL molecule pairs are placed on the Au electrode surface. This number of IL molecules is almost the same as or larger than in the previous studies.[30,38] The simulation box size along the *z* direction is 80 Å, which includes a vacuum region of ~25 Å. Note that the *z* coordinate is measured from the left-most layer of the electrode toward the bulk IL (see Figure 1).

All classical MD simulations for sampling IL configurations were performed by using the LAMMPS program package.[39] Temperature of IL molecules was controlled to be 300 K by the Nosé-Hoover thermostat algorithm.[40,41] Three dimensional periodic boundary conditions were applied, and long-range electrostatic interactions were calculated using the particle-particle particle-mesh Ewald scheme[42] with the Ewald surface term to model a pseudo-two dimensional system. Charges on each Au atom were set to zero for modeling the unbiased PZC condition. Other details including the employed force field information are described in Supplementary Information.

All first-principles electronic structure calculations were carried out on the basis of the density functional theory method by using the Quantum Espresso program package.[43] The exchange-correlation e•ect was taken into accounts within the Perdew-Burke-Ernzerhof (PBE) generalized gradient approximation.[44] This exchange-correlation functional has been used for reasonable descriptions of an Au slab and IL molecules and for estimates of interfacial potential drops.[18,29,36] According to the suggestion of previous studies[29,45-47], Grimme's dispersion correction method was used to treat the dispersion interaction in this study.[48,49] The Vanderbilt

ultrasoft-pseudopotential model[50] combined with a plane-wave basis set with 25 Ry cuto energy was used for describing the electronic structure as employed in previous studies.[51–53] The Brillouin-zone integrations were performed with a 2×2×1 Monkhorst-Pack k-point grid[54] except for geometry optimization calculations where only the Γ point was used. The 2×2×1 k-point grid with the $5\times3\sqrt{3}$ unit cell in the xy plane was confirmed, using a three-layer Au slab geometry, to give su ciently converged results of work function (5.28 eV, which gives accuracy of less than 0.01 eV compared to that in the 6×6×1 k-point grid). It should be noted that the computed work function (5.28 eV) is in good agreement with the experimental value (5.31 eV[24]). In the geometry optimization the positions of the Au electrode atoms at the left-most (or bottom) layer were fixed. All atoms except for the fixed atoms were optimized until the magnitude of the forces acting on them were less than 0.1 eV/Å. Although this convergence threshold is larger than that employed in other papers by a factor of 2-10,[17,19] the strict threshold is not necessary for our calculations because the present study focuses on the Au/IL structures at 300 K rather than zero temperature. The e ective screening medium method[55] was utilized to directly treat a non-repeated slab geometry in the surface normal direction. In order to obtain the reference level in the vacuum just outside the Au electrode (/IL molecules) systems, the simulation box edges were placed with a distance of 10 Å from the right- and left-most atoms. In the present paper the potential of the reference vacuum level was set to zero.

3 Results and Discussion:

3.1 Potential shift and PZC estimates: the largest contribution to the potential shift due to electron redistribution

Sampling of IL configuration and optimization of interfacial structure

We first performed classical MD simulations with the whole system and sampled 50 uncorrelated configurations of the IL molecules. The detail of the sampling procedure is described in Supplementary Information. Here we briefly show the remarkable points obtained from the sampling simulation: the distribution ratio of BMIM and TFSA molecules on the electrode surface and their qualitative adsorption structures. We found that BMIM and TFSA molecules evenly exist on the electrode surface (see Figure S3 in Supplementary Information for the computational evidence). This is reasonable because there are no electrostatic interactions between the Au electrode and the IL molecules (recall that the charges on each Au atom were set to zero for the PZC condition). Also note that the surface in the present system was fully covered by two IL pairs. BMIM molecules were observed to adsorb in a flat geometry with the imidazolium ring parallel to the surface. The butyl chain was also in direct contact with the surface, rather than pointing toward the IL bulk layer, in order to maximize the van der Waals interaction with the Au electrode. The BMIM molecules were also found to adsorb onto the surface without large flexible conformational and orientational changes. On the other hand, as for TFSA molecules at the surface, some conformations were observed in the sampled configurations. Those can be classified into the cis- and trans-conformations described in Ref. 29. The former has the two CF_3 groups both located above (or below) the S–N–S plane and the latter has conformations that one CF_3 group is above and the other is below the S–N–S plane. In the present simulation, the cis-type structure was found to be

the main conformation, where the oxygen atoms of the SO_2 groups are attached to the surface while the CF_3 groups point toward the direction opposite to the Au surface. These adsorption geometries of the BMIM and TFSA molecules are consistent with those shown in the previous experimental and theoretical studies.[29,56,57] In addition, we found that both IL molecules at the surface rarely switch the place with other molecules in the second IL layer. This indicates that there is the strong attractive interaction between the Au electrode and the IL molecules. The attractive interaction is described completely by the 12-6 LJ potential in the case of the present MD simulations, but we note that the effective LJ potential includes not only dispersion interaction but also other ones (such as polarization and charge transfer interactions) implicitly.

For the computationally e□cient estimate of the two contributions $\delta\Psi$ and $\delta\phi_{ele}$, we extract a partial system focused on the Au/IL interface from the whole system. The partial system includes the Au electrode and several IL molecules at the interface, but the size of that system may greatly a□ect the magnitude of the contributions. Thus, before the estimates of the contributions, we examined the dependence of the potential drop $\delta\phi_{ele}$ on the number of IL pairs at the surface in order to determine how many IL pairs are appropriate to estimate the contribution. Figure 2 shows the potential change profiles $\phi_{ele}(z)$ with one to six IL pair(s). (The interfacial structures used here are displayed in Figure S2 of Supplementary Information.) Note that the IL pairs were selected in order from the closer to the electrode surface. We found from the figure that two IL pairs are su□cient to estimate $\delta\phi_{ele}(= \phi_{ele}(z \sim -5\ \text{Å}) - \phi_{ele}(z \sim 18\ \text{Å}))$ at the qualitative and semi-quantitative levels. As mentioned above, the two IL pairs on the surface construct the first IL layer, which means the ~100 % monolayer coverage. This observation is consistent with the idea that electron polarization has the short-ranged

character. Although the potential contribution from $\delta\Psi$ is also influenced by the number of IL pairs, the dependence was estimated to be much smaller than that on $\delta\phi_{ele}$. Figure 2 was obtained from one sample configuration, but a similar trend was observed also for di□erent five samples from each other. We thus determined, for the estimates of the two contributions ($\delta\Psi$ and $\delta\phi_{ele}$), to use the partial systems including the whole electrode and two IL pairs in the first IL layer.

The partial system geometries extracted from the sampled configurations were next optimized at the first-principles calculation level. The IL molecules were relaxed to a locally stable geometry, so that no molecular orientation changes were observed. The most important geometrical aspect in this study is the relative z-positions of the Au atoms and the IL molecules at the interface because the variations are closely related to the electrostatic potential changes across the interface. Using the optimized 50 structures we calculated the average z-positions of characteristic atoms. Average z-position of Au atoms in the surface layer was found to shift by ~0.1 Å toward the fixed bottom layer upon adsorption of two IL pairs, in comparison to that of the bare Au electrode. The average distance along the *z* axis between the electrode surface layer and the N atoms of the BMIM molecules was estimated to be ~3.1 Å, which shows that the BMIM molecules come quite close to the electrode surface. The corresponding distances for the N and O atoms of the TFSA molecules were ~3.4 and ~2.9 Å, respectively. It has been reported from the first-principles MD calculations at 300 K that the average distance between the Au electrode surface and O atoms of water is ~4 Å.[33] Thus, the present result indicates that the TFSA molecules are located much closer to the electrode surface than water. The origin of the attractive force will be shown later (see Section 3.3).

Estimates of each potential change and resultant PZC

Now we start to show the results of the three potential change estimates. The contribution to the potential shift due to the geometrical modification of the electrode ($\delta\Psi$) was calculated according to Eq. 3. The obtained work function Ψ_{distM} was 5.14 eV on average. This is somewhat small compared with the work function of the bare Au electrode in vacuum (Ψ_M = 5.28 eV), which is consistent qualitatively with the destabilized electron potential caused by the distorted structure. The difference in work function between them leads to the potential downward shift by 0.14 V (i.e., $\delta\Psi/e_0$=–0.14 V, Table 1). From the small standard deviation of 0.01 V, we found that this contribution is quite insensitive to the IL configurations at the interface.

The contribution secondly considered is $\delta\phi_{ele}$ originating from the electron redistribution effect. According to Eq. 4, the value was estimated from the laterally averaged potential change upon adsorption

$$\phi_{ele}(z) = \phi^{Au/IL}(z) - \phi^{Au}(z) - \phi^{IL}(z), \quad (5)$$

where $\phi^{Au/IL}$, ϕ^{Au}, and ϕ^{IL} correspond to the potential profiles in the Au/IL partial system, the system including the Au electrode, and the system including the IL molecules, respectively. The resultant estimate was –0.74 V on average (Table 1 and Figure 3). This contribution works to shift the potential downwardly similar to $\delta\Psi$, but is much larger in magnitude than $\delta\Psi$. As shown in Figure 3, the potential changes greatly at the interface region between the electrode and the IL molecules and is lower in the electrode side than in the IL molecule side. From this observation, electron density is expected to increase in the electrode side rather than in the IL molecule side. The detailed analyses of this issue will be performed in the next section. As in the case of $\delta\Psi$, the small

standard deviation of ~0.04 V was obtained also for $\delta\phi_{ele}$, which shows the low sensibility to the IL configurations.

Finally, the remaining contribution coming from the orientation of the IL molecules $\delta\phi_{ori}$ was estimated by using all IL molecules extracted from the whole system. In this estimate, we carried out the first-principles calculations with only the Γ-point and no geometry optimizations. Considering the electronic insulation property of the IL molecules and the expectation that $\delta\phi_{ori}$ depends largely on the molecular macroscopic orientation rather than the fine structures such as bond distances and bond angles, this computational condition would be reasonable. Thus calculated potential drop was $\delta\phi_{ori}$= −0.07 V (Table 1). Although this potential drop across the IL region also contributes to the low potential, the magnitude is significantly small. Therefore, $\delta\phi_{ori}$ was found to be a minor contribution to the potential shift. Despite the near zero potential drop of $\delta\phi_{ori}$, we obtained here relatively larger standard deviation (~0.6 V) compared to the other two contributions. This indicates that each IL configuration has a somewhat charge-separated structure. However, the important point is that the charge-separated character mostly disappears by averaging their configurations. The fact implies that if a system with much larger xy surface area could be used for the estimate, such large potential deviation would be greatly reduced. Therefore, it is expected that the large deviation will not a・ect significantly the potential drop if uncorrelated configurations are sufficiently sampled. Note that the standard error of $\delta\phi_{ori}$ (~0.1 V) is su・ciently smaller than the magnitude of $\delta\phi_{ele}$.

Consequently, we estimated the potential shift ΔΨ(M=Au,S=IL) by summing up the obtained three contributions. The resultant shift was –0.95 V, which leads to the PZC of 4.33 V at the absolute scale. This is in good agreement with the experimental estimate

(4.1-4.5 V[25,26]). Among the interfacial potential changes considered here, that due to the electron redistribution was found to contribute dominantly to the negative potential shift. This finding suggests that the redistribution plays a crucial role to shift the potential of the Au electrode immersed in the IL.

3.2 Analyses of electron redistribution: electron transfer from IL molecules

We found from the above calculations that the electron redistribution at the Au/IL interface contributes dominantly to the negative potential shift from the work function to the PZC. This result implies that the electron distribution at the interface is polarized toward the electrode upon adsorption of the IL molecules. In order to make clear this speculation, in this section, we investigate the electron redistribution at the Au/IL interface in detail. Note that the following analyses were performed with an interfacial system containing the Au electrode and one IL pair in order to understand the mechanism more clearly. The essence of the mechanism is expected to be maintained even when the two or more IL pairs are placed on the surface, because the difference between their potential profiles $\phi_{ele}(z)$ is not qualitative but quantitative (see Figure 2). In addition, it was confirmed that the conclusions derived below do not change even if other IL configurations sampled in the MD simulations are used for the analyses.

Electron density change

Although we showed the potential profile $\phi_{ele}(z)$ in the previous section, we can also show directly the electron density change associated with the IL adsorption

$$\rho_{ele}(z) = \rho^{Au/IL}(z) - \rho^{Au}(z) - \rho^{IL}(z), \quad (6)$$

where $\rho^{Au/IL}$, ρ^{Au}, and ρ^{IL} are the electron densities along the z direction in the Au/IL partial system, the system including the Au electrode, and the system including the IL molecules, respectively. This is analogous to Eq. 5. Figure 4 displays $\rho_{ele}(z)$ as well as

the electron densities $\rho^{Au/IL}$, ρ^{Au}, and ρ^{IL}. The figure clearly shows that the electron density on the electrode side increases while that near the IL molecules decreases. This indicates that the electrode surface is negatively charged and the IL molecules are positively charged on average. From the figure, we can see the electron transfer from the IL molecules to the electrode, but it is difficult to see which IL molecule releases its electron because the electron density change $\rho_{ele}(z)$ is averaged within the xy plane. We thus plotted the density change in the three dimensional form (Figure 5). The regions where the electron density increases (decreases) are represented by red (blue) colored isosurfaces. A qualitative view shows that the regions where the electron density increases are mainly located at the electrode surface adsorbed by the BMIM molecule, while the regions where it decreases are broadly located at the BMIM molecular surface closer to the electrode, the entire TFSA molecule, and the electrode surface adsorbed by the TFSA molecule. It seems that the both BMIM and TFSA molecules release their electron to the electrode surface, in particular though the BMIM molecule is already positively charged. (Note that we confirmed that the BMIM and TFSA molecules are positively and negatively charged by about 1 e_0, respectively, by calculating dipole moment with the system containing only the IL molecules.) From a different viewpoint, the electron density change at the electrode surface may be regarded as the image charges induced by the ionic molecules. This polarization takes place in the same direction as the dipole moment of the IL molecule pair. Similar electron redistribution within the electrode surface has been observed also in the Ag(111) surface adsorbed by an IL molecule pair.[29]

We found that the electron redistribution manner is greatly different between around the BMIM cation and the TFSA anion. We thus re-plotted the electron density

change along the z direction (Figure 6), but the averaging in the xy plane was performed in a di□erent manner from that used in Figure 4. Here, the whole plane was partitioned into two regions according to the green line in Figure 5a. As can be seen from the figure, this dividing surface perpendicular to the xy plane well partitions the spaces associated with the two IL molecules.[58] Red and green lines in Figure 6 represent the electron density changes in the region associated with the BMIM and TFSA molecules, respectively, and the sum of them is plotted by blue color. Note that the blue-colored line is identical to the plot in Figure 4. The increase in electron density at the electrode surface (z ~5-6 Å) was found to appear as a result of two opposite signed ρ_{ele}'s associated with the BMIM and TFSA regions. The decrease in electron density at the IL molecular side shows a somewhat di・erent character between the two molecules. The BMIM region displays the large electron depletion at the molecular surface facing on the electrode (z~7 Å) and the small electron enhancement and depletion at z~7.5-10.0 Å. The former obviously shows the electron transfer to the electrode surface, whereas the latter would be reasonable to be regarded as the intramolecular electron polarization. On the other hand, in the TFSA region, we can see the electron depletion in the entire of the TFSA molecule (z~7-12 Å). The broad electron depletion may be related to the anionic character of the TFSA molecule with an excess electron. We, therefore, suggest that the electron redistribution toward the electrode takes place from both the TFSA and BMIM molecules.

Density of states

We also examined the electron redistribution in terms of density of states (DOS). Although analyses using DOSs are based on the one-electron picture, they are very useful to understand the electronic structure qualitatively. Figure 7a shows the projected

DOSs (p-DOSs) onto the atomic orbitals involved in the BMIM. Red and green plots correspond to the p-DOSs of the system containing only the IL pair and both the electrode and the IL pair, respectively. Reflecting the electronic character of the isolated IL molecules, the p-DOS calculated in the system without the electrode has an energy gap between the highest occupied molecular orbital (MO) at ~–7.8 eV and the lowest unoccupied MO at ~–3.2 eV. When the electrode was introduced to the IL system, the overall structure of the p-DOS significantly changed. In particular, the energy gap observed in the IL system was found to disappear. This is a result of the interaction between MOs of the BMIM molecule and bands of the Au electrode. The p-DOS was further projected onto the occupied and unoccupied MOs of the BMIM molecule using the method proposed by Ravikumar and coworkers[59] (Figure 7b). The figure shows that the contribution of the BMIM occupied MOs (red line) penetrates into the conduction band region. This structure clearly suggests that a small amount of electron is removed from the BMIM molecule and the occupied MO partially has the unoccupied character. In addition, we also found that the highest occupied MO, which is the π orbital extending over the entire imidazolium ring, contributes to the electron transfer the best (see Supplementary Information for details). Contrary to the occupied MOs, the unoccupied MOs are shown to contribute little to the valence bands (green line in Figure 7b), indicating that there are little electron transfer from the Au electrode to the BMIM molecule. This is a result of avoiding an unstable state caused by occupying the high-lying MOs. These observations lead to the conclusion that the BMIM interacts with the electrode in a chemical manner involving the electron transfer from the molecule, which is clearly consistent with the observation in the electron density analysis described above. Also for the TFSA molecule, the calculated p-DOSs provided

qualitatively the same observations as for the BMIM molecule (see Figure S4 of Supplementary Information).

Effect of BMIM orientation on electron redistribution

In order to gain further evidence, we performed additional calculations with two systems where a BMIM molecule has distinctly di□erent orientations from that shown above (i.e., parallel orientation to the electrode surface). One has an imidazolium-ring orientation perpendicular to the electrode surface and the other has a tilted imidazolium-ring orientation with distance from the electrode surface (see Figure 8a and b, respectively). Although the TFSA configurations are not the same as each other, the difference is confirmed not to critically influence the electron redistribution associated with the BMIM (see Figure S5 in Supplementary Information). The obtained results are displayed in Figure 8c and d. The electron density change profiles, which were plotted in the same manner as in Figure 6, show qualitatively the same result, i.e., the electron depletions at the BMIM molecular surface (z~7 Å) are significantly mitigated compared with that in the BMIM parallel orientation (Figure 6). These plots indicate that the electron transfer from the BMIM molecule does not take place to a large extent. We can observe the trend also from the MO-projected DOSs (Figure S6 of Supplementary Information). As a result, the potential change due to the electron redistribution $\delta\phi_{ele}$ was estimated to be −0.37 and −0.15 V for the BMIM orientations of Figure 8a and b, respectively (see Table S1 in Supplementary Information). These values are smaller in magnitude than that obtained in the parallel orientation case (−0.51 V, see Figure 2). With these additional calculations, we successfully obtained the solid evidence about the electron transfer from the cationic BMIM molecule.

3.3 Discussion

Electronic charge change and origin of electron transfer

In the previous sections we investigated the mechanism on the electron redistribution caused by the IL adsorption in detail. We concluded that the redistribution corresponds to the electron transfer from the IL molecules to the Au electrode surface. Here an intriguing question is how much the amount of electron is released from the IL molecules. As mentioned in Introduction, there is a report by Buchner and coworkers of the charge analysis[29], suggesting that the charges of the IL molecules hardly change upon adsorption. In order to answer the question, we roughly estimated the electronic charge by integrating $\rho_{ele}(z)$ along the z axis. The obtained charge in the electrode side[60] was about −0.4 e_0 on average, which corresponds roughly to the release of about only 0.1 electron for each IL molecule. (Note that the analysis was performed with the systems including two IL pairs.) This result seems not far from the previous report. The relatively small electron transfer may be due to the fact that the electron transfer is unfavorable in terms of the energy alignment of the relevant orbitals. As found from Figure 7a and the work function of the bare Au (~5.3 eV), there is a rather large energy gap (> 2 eV) between the highest occupied MO of the BMIM and the lowest conduction band of the Au electrode. This large gap significantly inhibits the electron transfer from the occupied MOs to the conduction bands. Even so, however, it is certain that the electron transfer was observed. This can be explained by the sufficiently large electronic coupling between the electrode and the IL molecules. Given that the coupling scales with the overlap of the interacting orbitals, it is reasonable to consider that the observed

small electrode-molecule distance (see Section 3.1) gives a large orbital overlap and consequently leads to a sufficient electronic coupling. In addition, the large coupling is also expected to come from the high Au d-band DOSs ranging from –12 to –6 eV and its tail up to around Fermi level. Overall, therefore, we argue that the small electron transfer causes the large potential change at the electrode-IL interface.

According to the small electronic charge change, the attractive electrostatic interaction associated with the electron transfer is unlikely to give such a closely approached Au/IL interfacial structure. What is the origin of such characteristic structures? We gained an answer from the adsorption energy calculation that it is the dispersion interaction. We obtained the adsorption energy of −7.3 eV per two IL pairs, which was confirmed to be attributed almost-totally to the dispersion interaction (see Supplementary Information for details). This result is consistent with the previous calculations of Buchner and coworkers[29]. In fact, without the dispersion correction, the distance between the electrode surface and the IL molecules became larger by ~0.7 Å compared to that with the dispersion interaction (within the present convergence threshold in geometry optimization), resulting in the almost vanished adsorption energy (~0.2 eV). Besides, as expected, the potential change of $\delta\phi_{ele}$ decreased to −0.32 V, which is less than the half in magnitude of displayed value above (see Table 1). Therefore, we suggest that the large potential shift investigated here originates from the strong dispersion interaction between the electrode and the molecules at the interface. This might be similar to the suggestion that the physical adsorption due to the

dispersion interaction can be a precursor to the chemical adsorption involving some charge transfer processes.[61–63]

Here we should note that the important factor to generate such potential shift may alter in the case of biased electrodes. In general, a biased electrode with excess charges is able to attract IL molecules via electrostatic interaction, too. Also in such cases, if an interfacial structure with a small electrode-IL molecule distance is constructed, the electron transfer generating the potential drop is expected to occur. Therefore, for understanding the potential change by the electron redistribution, it is critical to focus on the interfacial structure that adsorbates approach sufficiently closely to the electrode surface, rather than a strong dispersion attraction itself. Besides, the IL orientation effect, which was estimated to be small in the unbiased condition, may show a non-negligible contribution to the potential shift because of a highly-ordered electrical double layer of IL molecules.

Implication for the potential shift of other kinds of metal/IL systems

In this paper we have addressed the potential shift of the Au electrode caused by the [BMIM][TFSA] IL molecules. The choice of this system has been motivated by the experimental study of Motobayashi and coworkers[25]. However, other kinds of metal electrodes are routinely used in electrochemical experiments. In particular, the Pt electrode attracts much attention in many fields as a promising material. First-principles calculations showed the binding strength between a metal and water molecules is ordered according to Au < Ag < Cu < Pd < Pt for some typical late transition metals[64], indicating the relatively inactive Au electrode surface. It was also shown by other first-principles calculations that the potential shift caused by the electron redistribution in the Pt/water system is more than doubled compared to that in the Au/water system[18].

On the basis of these computational results, metal/IL systems with relatively active electrode surface such as the Pt electrode may show a larger potential shift in magnitude than the corresponding Au system due to the stronger binding of IL molecules.

On the other hand, IL is well known as a highly-tunable electrolyte to attain some desired properties. The potential shift and the resultant PZC are also expected to be influenced by the combinations of anion and cation molecules as other properties are. As described above, the potential shift under the PZC condition originates mainly from the dispersion interaction forming a short-distanced interfacial structure. The BMIM cation is one of the molecules expected to have relatively large dispersion interaction owing to its large contact surface area and π orbital on the imidazolium ring. For example, if the cation was replaced with a spherical one such as an ammonium NR_4^+, what would happen in terms of the electrode potential shift? Because the spherical cations are expected to contact with the flat electrode surface through a relatively small area, the dispersion interaction between them would become rather weak. Consequently, it is supposed to generate a smaller potential shift than that presented in this study. This would be applied also to anions.

Although the above inferences are expected to partly capture the actual interaction at the interface, it is also true that they are crude predictions. Since the interaction between a metal electrode and electrolyte molecules must be more complicated, it is difficult to correctly predict the potential shift of other systems using limited data. Besides, we need to consider other effects, such as energy alignment and electrical double layer structures, for the correct prediction. To our knowledge, there are no reports which explain the system dependence of the potential shift, yet. To understand the complicated relationship between the system and the potential shift, systematic

investigations based on the theoretical approaches like this study are expected to be a promising way allowing to direct comparison of the potential shifts without experimental error. Such investigations will lead eventually to a practical technology which tunes finely the potential shift by modifying the system components.

Comparison with the metal/water system and importance of ensemble average of molecular configuration

As mentioned in Introduction, many previous studies have focused on the potential shift of metal electrodes in water. Schnur and Groß have reported the potential shift of –0.6 V in the Au/water system.[33] Le and coworkers have also showed the quantitatively similar result.[18] This negative shift agrees qualitatively with that in the present IL case. In addition, we found that the mechanism that the electron redistribution has a dominant contribution to the negative potential shift is the same in both water and IL cases. However, there is a notable di□erence between them. Water molecules in the first layer change the orientation easily due to the weak interaction with Au electrode atoms and the molecules which have the specific orientation contribute dominantly to the potential shift through the electron transfer[18, 33]. Thus, for the adequate estimate of the potential shift, it is critically important to take into account the ensemble of water configurations at the interface. On the other hand, in the case of the present IL molecules, the orientation change linked to the electron transfer rarely occurs in particular for the BMIM molecule, because of the strong interaction between the molecules and the electrode. This is reflected in the small standard deviation of $\delta\phi_{\mathrm{ele}}$ ($\sim$0.04 V). Accordingly, in the estimate of the potential shift stemmed from the electron redistribution, the ensemble average may be less important in the case of electrolyte molecules like BMIM which strongly bind to the electrode surface.

4 Conclusion and Outlook:

In this paper we investigated the mechanism on the potential shift of the Au electrode upon immersing into the [BMIM][TFSA] IL using the first-principles calculations. Firstly, we successfully obtained the potential shift, which was supported by the computational PZC consistent with the experimental value. It was shown that the electron redistribution at the Au/IL interface has a dominant contribution to the potential shift. The interfacial electron redistribution was then deeply investigated and, as a result, the redistribution was found to correspond to the electron transfer from the IL molecules to the electrode surface. Importantly, it occurs not only from the anionic TFSA molecule but also from the cationic BMIM molecule. It was also found that the electron transfer is small quantitatively and its associated interaction contributes little to the adsorption energy compared to the dispersion interaction. Nevertheless, it is emphasized to play a non-negligible role in the potential shift. We finally concluded that this unexpected and interesting observation originates from the strong adsorption of the molecules on the electrode surface by the dispersion interaction. On the basis of the findings we propose that the electron transfer leading to the potential shift may often occur in adsorbates which very closely approach to an electrode even if the adsorbate is a cationic molecule. The obtained insights are useful for understanding electrochemical phenomena at metal/IL interfaces.

In the present study we focused on the potential of the unbiased Au electrode immersed into the [BMIM][TFSA] IL. However, experiments use various kinds of metal or semiconductor electrodes combining with a variety of IL, and many electrochemical processes take place under the biased electrode conditions. Although

some inferences related to the issues were given in this paper, deep investigations for various systems and electrochemical conditions are left for future studies.

Conflicts of interest:

There are no conflicts to declare.

Acknowledgements:

This research was mainly supported by the programs of the Ministry of Education, Culture, Sports, Science and Technology (MEXT) in Japan; ”Priority Issue on Post-K computer” (Development of new fundamental technologies for high-e□ciency energy creation, conversion/storage and use) using computational resources of the K computer provided by the RIKEN Center for Computational Science through the HPCI System Research project (Project ID: hp170241) and “Elements Strategy Initiative for Catalysts and Batteries (ESICB)”; by the Core Research for Evolutional Science and Technology (CREST) of the Japan Science Technology Agency (JST); and also by a Grant-in-Aid for Science Research from MEXT. The computations were also performed using Research Center for Computational Science, Okazaki, Japan and also using several computing systems at the Information Technology Center in Nagoya University, Japan. Molecular figures were created with VMD.[65]

Notes and references:

1. W. Schmickler, *Chem. Rev.,* 1996, **96**, 3177–3200.
2. A. N. Frumkin, O. A. Petrii, B. B. Damaskin, *Comprehensive Treatise of Electrochemistry: The Double Layer*, Springer US, 1980, pp 221–289.
3. M. Grdeń, M. Łukaszewski, G. Jerkiewicz, A. Czerwiński, *Electrochim. Acta,* 2008, **53**, 7583–7598.
4. A. G. Silva, N. Bundaleski, A. M. C. Moutinho, O. M. N. D. Teodoro, *Appl. Surf. Sci.*, 2012, **258**, 2006-2009.
5. M. Oertel, M. Schulze, M. V. Bradke, W. Schnurnberger, *Ber. Bunsenges. Phys. Chem.*, 1993, **97**, 360-362.
6. S. Sakong, K. Forster-Tonigold, A. Groß, *J. Chem. Phys.*, 2016, **144**, 194701.
7. R. P. Janek, W. R. Fawcett, A. Ulman, *J. Phys. Chem. B*, 1997, **101**, 8550–8558.
8. J. Poon, C. Batchelor-McAuley, K. Tschulik, R. G. Compton, *Chem. Sci.*, 2015, **6**, 2869–2876.
9. D. M. Adams, L. Brus, C. E. D. Chidsey, S. Creager, C. Creutz, C. R. Kagan, P. V. Kamat, M. Lieberman, S. Lindsay, R. A. Marcus, et al., *J. Phys. Chem. B*, 2003, **107**, 6668–6697.
10. A. Bhaskar, M. Deepa, T. N. Rao, *ACS Appl. Mater. Interfaces* 2013, **5**, 2555–2566.
11. S. Trasatti, *In Advances in Electrochemistry and Electrochemical Engineering*, Wiley Interscience, 1977, 10.
12. V. V. Emets, B. B. Damaskin, *Russ. J. Electrochem.*, 2009, **45**, 45–57.
13. J. O. Bockris, S. D. Argade, *J. Chem. Phys.*, 1968, **49**, 5133–5134.
14. S. Trasatti, *J. Electroanal. Chem. Interfacial Electrochem.*, 1986, **209**, 417–428.
15. J. Cheng, M. Sprik, *Phys. Chem. Chem. Phys.*, 2012, **14**, 11245–11267.

16. J. Kaur, R. Kant, *J. Phys. Chem. C*, 2017, **121**, 13059–13069.

17. R. Jinnouchi, A. B. Anderson, *Phys. Rev. B*, 2008, **77**, 245417.

18. J. Le, M. Iannuzzi, A. Cuesta, J. Cheng, *Phys. Rev. Lett.*, 2017, **119**, 016801.

19. V. Tripkovic, M. E. Björketun, E. Skúlason, J. Rossmeisl, *Phys. Rev. B*, 2011, **84**, 115452.

20. A. Cuesta, *Surf. Sci.*, 2004, **572**, 11–22.

21. T. Welton, *Chem. Rev.*, 1999, **99**, 2071–2084.

22. P. Simon, Y. Gogotsi, *Nat. Mater.*, 2008, 7, 845–854.

23. A. Lewandowski, A. Świderska-Mocek, *J. Power Sources*, 2009, **194**, 601–609.

24. H. B. Michaelson, *J. Appl. Phys.*, 1977, **48**, 4729–4733.

25. K. Motobayashi, K. Minami, N. Nishi, T. Sakka, M. Osawa, *J. Phys. Chem. Lett.*, 2013, **4**, 3110–3114.

26. The experimental electrode potential had been indicated at the Fc/Fc+ scale. For conversion to the absolute scale, a relation of 0 V vs Fc/Fc+ = 0.4-0.8 V vs standard hydrogen electrode and the absolute standard hydrogen electrode potential of 4.44 V were used.

27. V. O. Santos, M. B. Alves, M. S. Carvalho, P. A. Z. Suarez, J. C. Rubim, *J. Phys. Chem. B*, 2006, **110**, 20379–20385.

28. S. Baldelli, *Acc. Chem. Res.*, 2008, **41**, 421–431.

29. F. Buchner, K. Forster-Tonigold, B. Uhl, D. Alwast, N. Wagner, H. Farkhondeh, A. Groß, R. J. Behm, *ACS Nano*, 2013, **7**, 7773–7784.

30. E. Paek, A. J. Pak, G. S. Hwang, *J. Chem. Phys.*, 2015, **142**, 024701.

31. Y. Ando, Y. Gohda, S. Tsuneyuki, *Chem. Phys. Lett.*, 2013, **556**, 9–12.

32. D. Cornil, T. Van Regemorter, D. Beljonne, J. Cornil, *Phys. Chem. Chem. Phys.*,

2014, **16**, 20887–20899.

33. S. Schnur, A. Groß, *New J. Phys.*, 2009, **11**, 125003.
34. C. D. Taylor, S. A. Wasileski, J.-S. Filhol, M. Neurock, *Phys. Rev. B*, 2006, **73**, 165402.
35. L. Börnstein, *Numerical data and functional relationships in science and technology, Crystal and Solid State Physics*, ed. O. Madelung (Springer, Berlin, 1984), 17a.
36. Y. Ando, Y. Kawamura, T. Ikeshoji, M. Otani, *Chem. Phys. Lett.*, 2014, **612**, 240–244.
37. M. Otani, I. Hamada, O. Sugino, Y. Morikawa, Y. Okamoto, T. Ikeshoji, *J. Phys. Soc. Jpn.*, 2008, **77**, 024802.
38. K. Ma, X. Wang, Y. Cui, F. Lin, C. Deng, H. Shi, *Chem. Phys. Lett.*, 2017, **677**, 137–142.
39. S. Plimpton, *J. Comput. Phys.*, 1995, **117**, 1–19, http://lammps.sandia.gov.
40. S. Nosé, *Mol. Phys.*, 1984, **52**, 255–268.
41. W. G. Hoover, *Phys. Rev. A*, 1985, **31**, 1695–1697.
42. R. W. Hockney, J. W. Eastwood, *Computer Simulation Using Particles*, Taylor & Francis Group, 1988.
43. P. Giannozzi, S. Baroni, N. Bonini, M. Calandra, R. Car, C. Cavazzoni, D. Ceresoli, G. L. Chiarotti, M. Cococcioni, I. Dabo, et al., *J. Phys.: Condens. Matter*, 2009, **21**, 395502.
44. J. P. Perdew, K. Burke, M. Ernzerhof, *Phys. Rev. Lett.*, 1996, **77**, 3865–3868.
45. K. Tonigold, A. Groß, *J. Chem. Phys.*, 2010, **132**, 224701.
46. K. Tonigold, A. Groß, *J. Comput. Chem.*, 2012, **33**, 695-701.
47. T. Waldmann, C. Nenon, K. Tonigold, H. E. Hoster, A. Groß, R. J. Behm, *Phys.*

Chem. Chem. Phys., 2012, **14**, 10726.

48. S. Grimme, *J. Comput. Chem.*, 2006, **27**, 1787–1799.
49. V. Barone, M. Casarin, D. Forrer, M. Pavone, M. Sambi, A. Vittadini, *J. Comput. Chem.*, 2009, **30**, 934–939.
50. D. Vanderbilt, *Phys. Rev. B*, 1990, **41**, 7892–7895.
51. G. Cicero, A. Calzolari, S. Corni, A. Catellani, *J. Phys. Chem. Lett.*, 2011, **2**, 2582–2586.
52. M. Hoefling, F. Iori, S. Corni, K.-E. Gottschalk, *Chem. Phys. Chem.*, 2010, **11**, 1763– 1767.
53. N. Mammen, S. Narasimhan, S. de Gironcoli, *J. Am. Chem. Soc.*, 2011, **133**, 2801–2803.
54. H. J. Monkhorst, J. D. Pack, *Phys. Rev. B*, 1976, **13**, 5188–5192.
55. M. Otani, O. Sugino, *Phys. Rev. B*, 2006, **73**, 115407.
56. E. S. C. Ferreira, C. M. Pereira, M. N. D. S. Cordeiro, D. J. V. A. dos Santos, *J. Phys. Chem. B*, 2015, **119**, 9883-9892.
57. T. Cremer, M. Stark, A. Deyko, H.-P. Steinrck, F. Maier, *Langmuir*, 2011, **27**, 3662–3671.
58. The line was drawn so as to partition well the isosurface of electron density change into each molecule. The arbitrariness of the partitioning may lead to somewhat artificial results, but it was confirmed that qualitatively the same results as Figure 6 can be obtained with four di□erent IL configurations.
59. A. Ravikumar, A. Baby, H. Lin, G. P. Brivio, G. Fratesi, *Sci. Rep.*, 2016, **6**, 24603.
60. We partitioned the integrated charge into the electrode and IL molecular sides by using a plane which is parallel to the electrode surface and includes the middle point

between the surface and the adsorbed BMIM molecular plane.

61. K. Prince, G. Paolucci, A. Bradshaw, *Surf. Sci.*, 1986, **175**, 101–122.

62. C. R. Henry, C. Chapon, C. Duriez, *J. Chem. Phys.*, 1991, **95**, 700–705.

63. Y. Yourdshahyan, A. M. Rappe, *J. Chem. Phys.*, 2002, **117**, 825–833.

64. A. Michaelides, *Appl. Phys. A*, 2006, **85**, 415-425.

65. W. Humphrey, A. Dalke, K. Schulten, *J. Molec. Graphics* 1996, **14**, 33–38.

Table 1: Computed work function Ψ_{Au} (eV), three contributions to the potential shift, $\delta\Psi/e_0$, $\delta\phi_{ele}$, and $\delta\phi_{ori}$ (V), and resultant PZC (V).

Ψ_{Au}	$\delta\Psi/e_0$	$\delta\phi_{ele}$	$\delta\phi_{ori}$	PZC
5.28	−0.14(0.001)[a]	−0.74 (0.01)[a]	−0.07 (0.09)[a]	4.33 (0.10)[a]

Experimental work function of Au(111) and the PZC at the absolute scale are 5.31 eV[24] and 4.1-4.5 V[25], respectively.

[a] The value in parenthesis represents standard error.

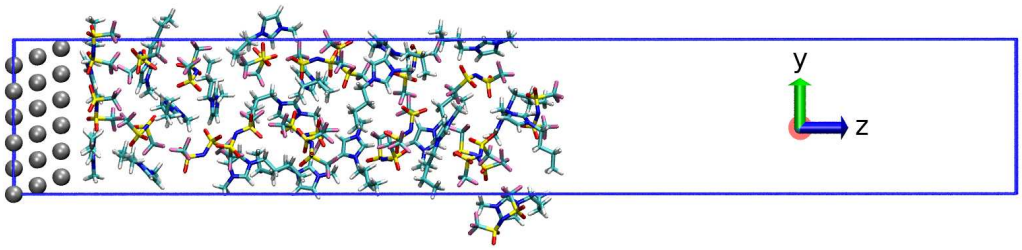

Figure 1: Simulation box containing a three-layered Au electrode and 20 [BMIM][TFSA] ion pairs. The z axis corresponds to the normal direction to the electrode surface. Three dimensional periodic boundary conditions are applied for classical MD simulations.

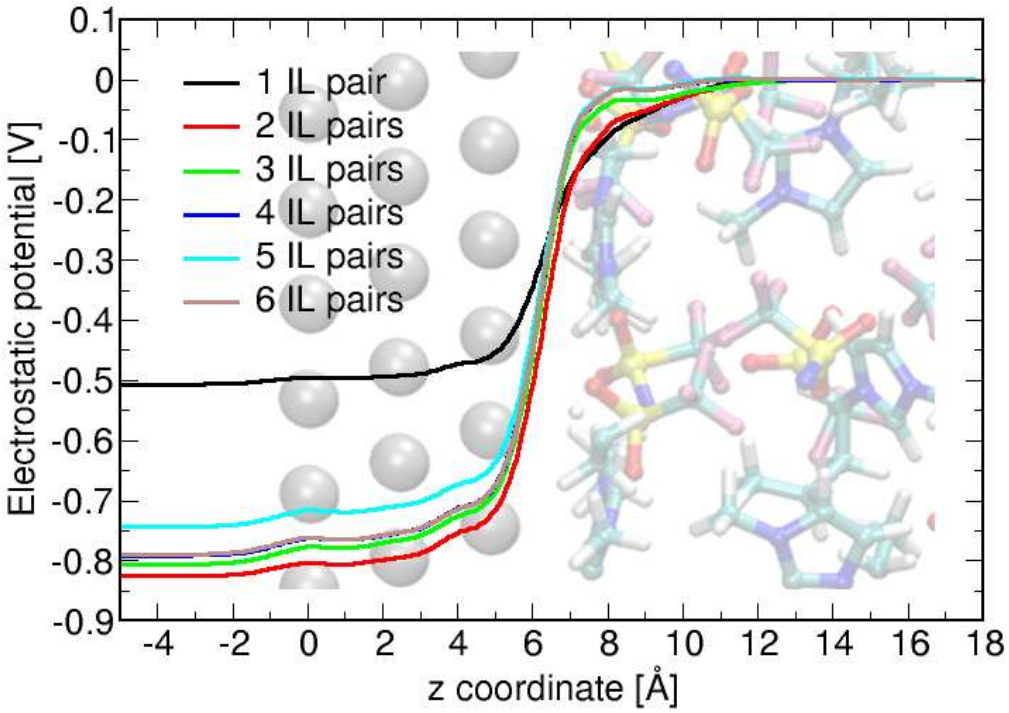

Figure 2: Potential change profiles $\phi_{ele}(z)$ due to the adsorption of one to six IL pairs on the electrode surface.

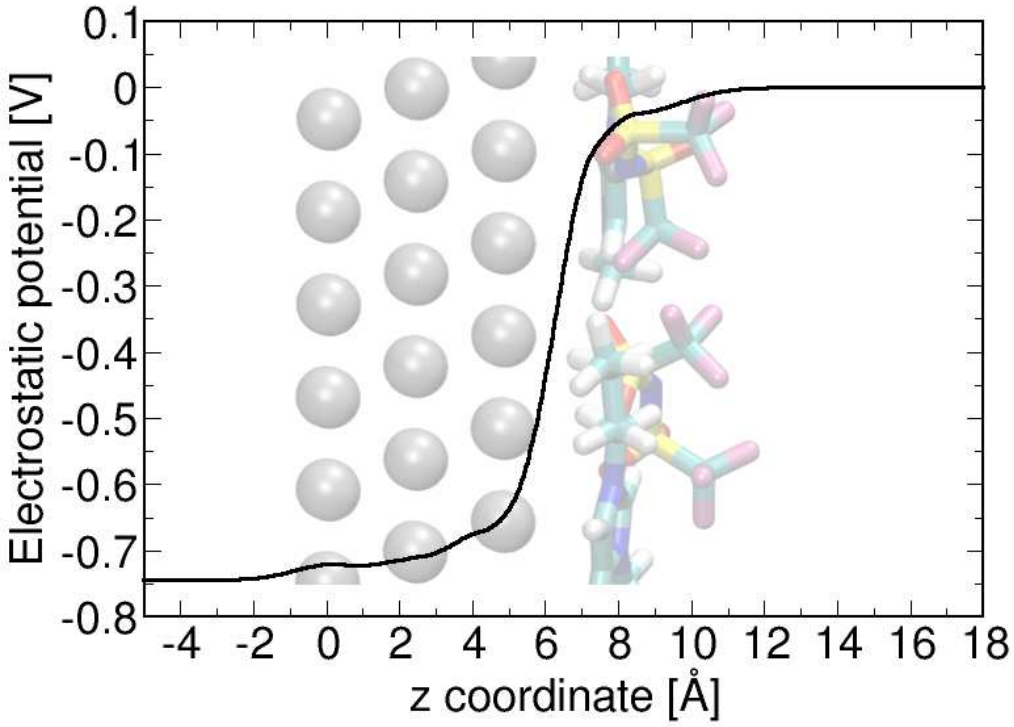

Figure 3: Averaged potential change profile $\phi_{ele}(z)$ calculated with 50 IL configurations.

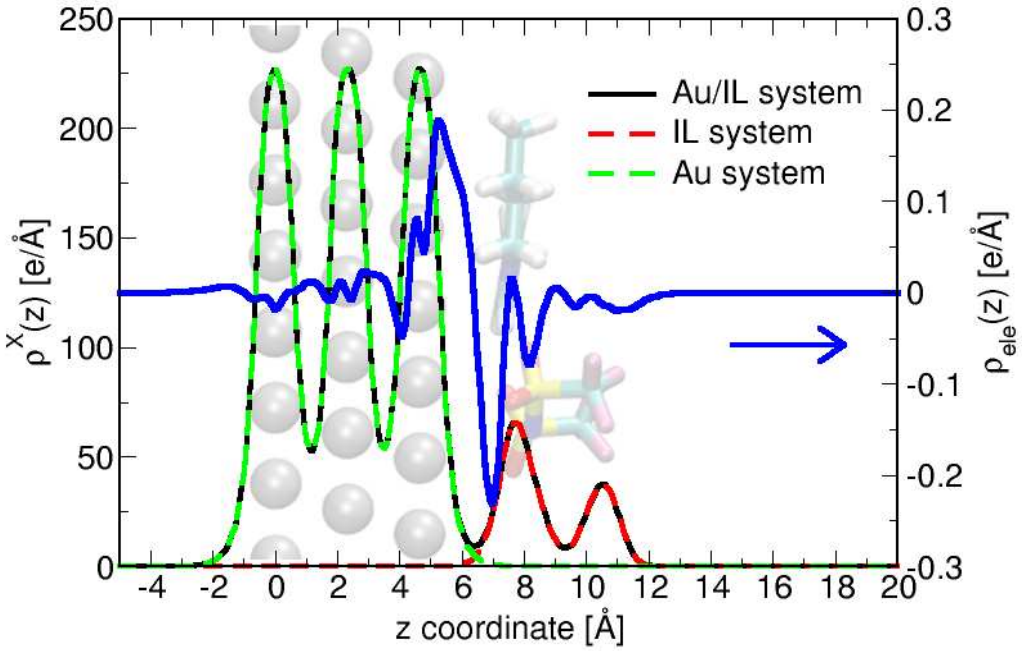

Figure 4: Electron densities ρ^X of the systems including both the electrode and the IL pair (black line, X=Au/IL), the electrode (green dashed line, X=Au), and the IL pair (red dashed line, X=IL), and the electron density change caused by the adsorption of the IL pair (ρ_{ele}, which is represented by blue line). Note that the electron density change is plotted with the right axis.

(a)

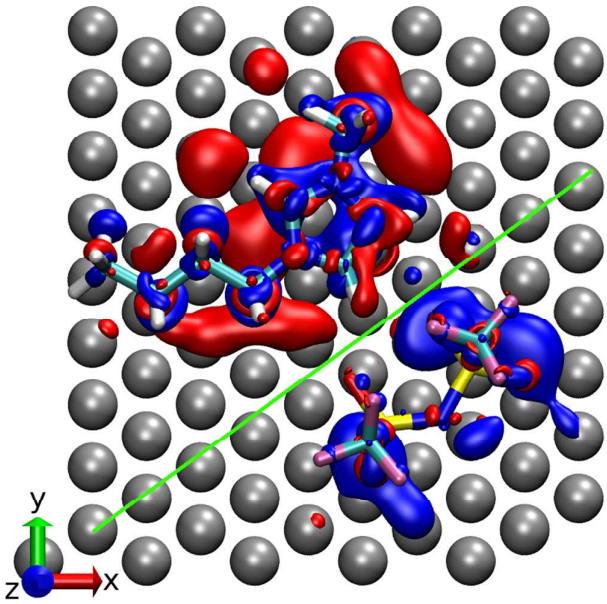

(b)

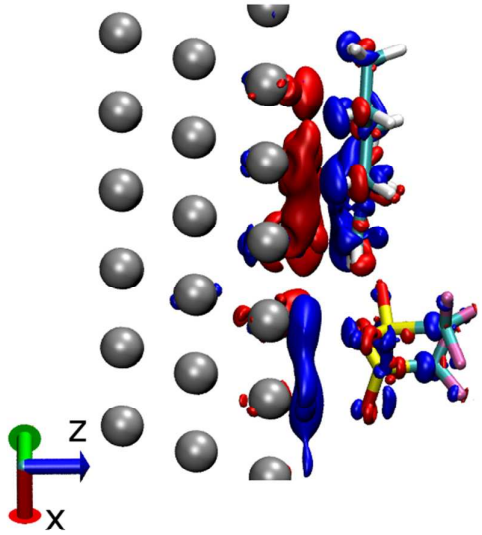

Figure 5: Three dimensional isosurfaces of electron density change due to the adsorption of the IL pair ($\pm 1.2\times10^{-5}$ e/Å^3). Red and blue isosurfaces indicate the increasing and decreasing regions of electron, respectively. Panel (a) and (b) are top and side views of the Au/IL system, respectively. Green line in the panel (a) shows a dividing surface used in Figure 6, see the text for details.

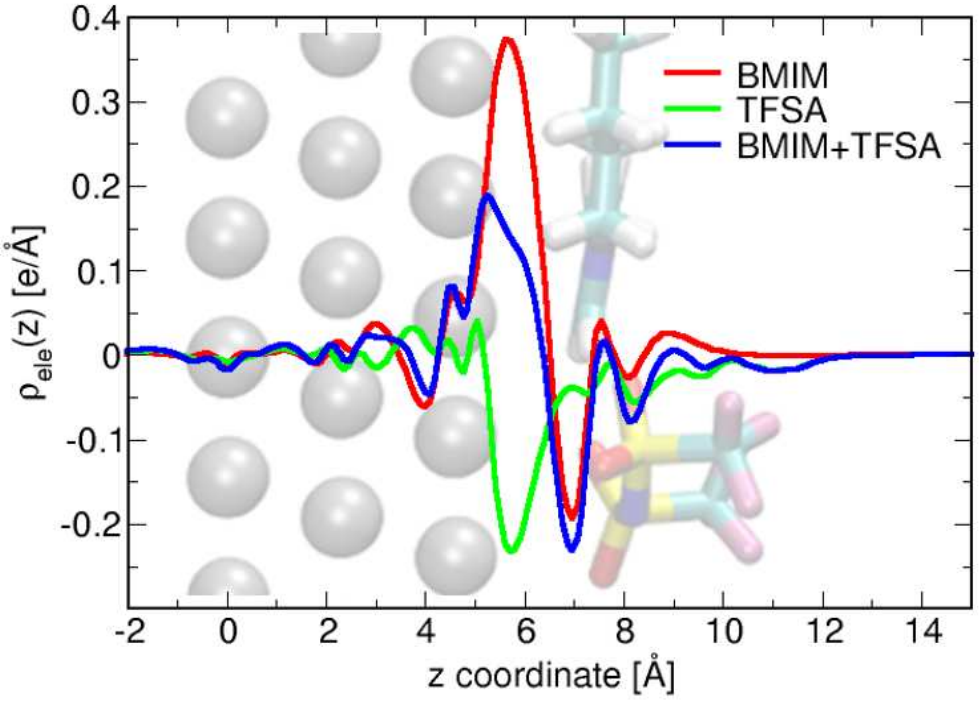

Figure 6: Electron density changes obtained by partitioning the three dimensional plot into the region associated with each IL molecule. Red and green lines show the changes in the regions associated with the BMIM and TFSA molecules, respectively. The blue line is the sum of them.

(a)

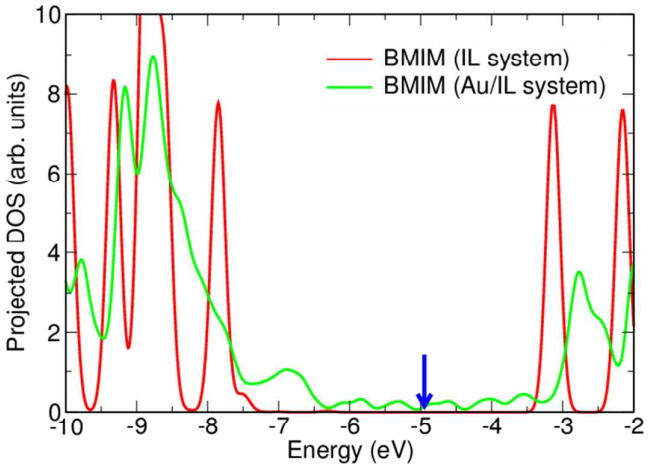

(b)

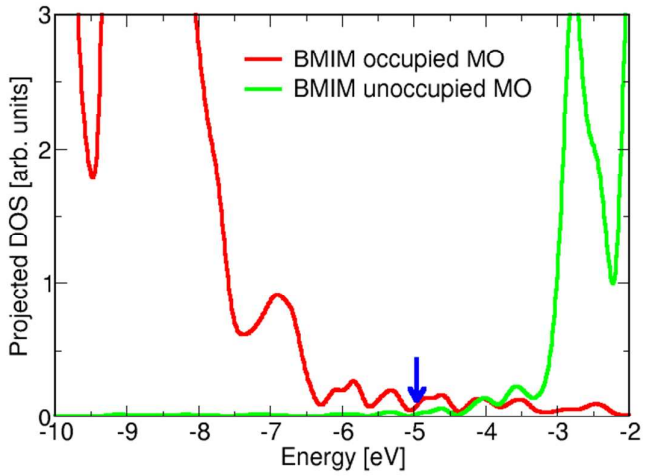

Figure 7: Panel (a): projected densities of states on the BMIM molecule in the isolated IL pair (red line) and the Au/IL system (green line). Panel (b): molecular orbital (MO) projected DOSs. Red and green lines represent, respectively, the contributions from the BMIM occupied and unoccupied MOs. Blue arrows indicate the Fermi level in the Au/IL system. Energy zero is set to the vacuum level outside the IL molecules.

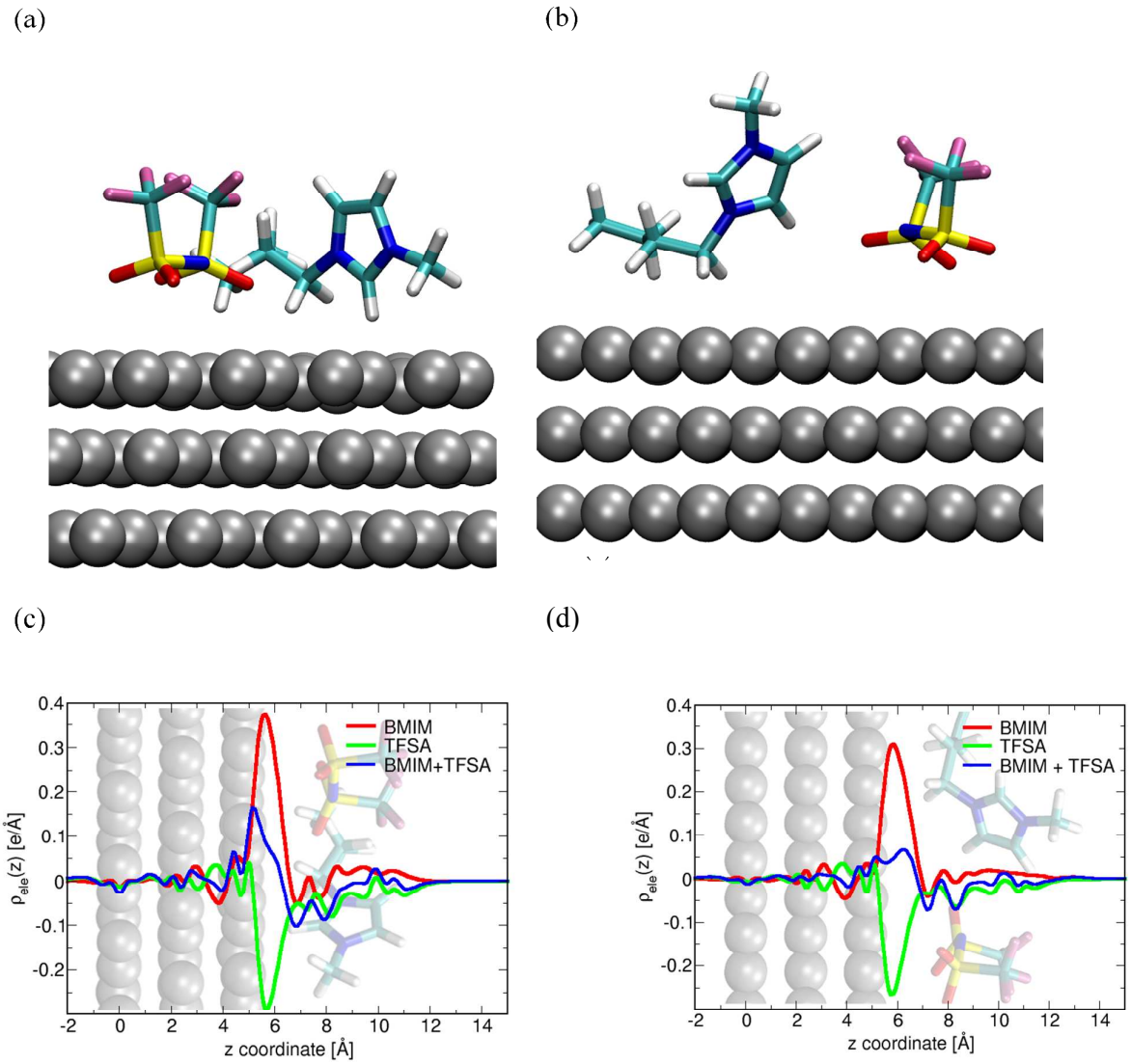

Figure 8: Molecular structure (a) and electron density changes (c) for the system with an imidazolium-ring orientation perpendicular to the electrode surface. Panels (b) and (d) correspond, respectively, to ones for the system with a tilted imidazolium-ring orientation with a distance from the electrode surface.

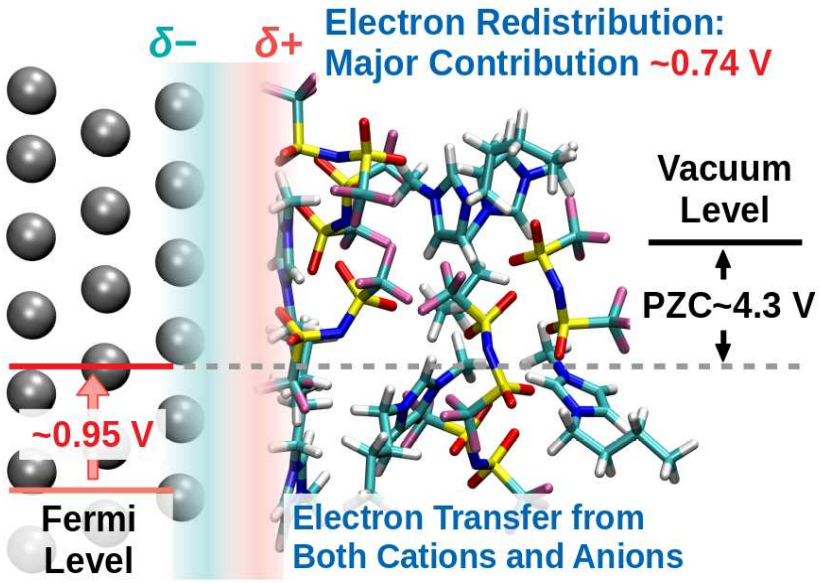

Table of Contents Graphics:
Electron transfer from both cations and anions to the Au surface contributes dominantly to the electrode potential shift.